

Design and Fabrication of working Pockels-Effect EO Polymer Modulators as Novice Designers.

Davin Birdi

Contact: dbirdi@student.ubc.ca

Department of Electrical and Computer Engineering
University of British Columbia, Vancouver, BC V6T 1Z4, Canada

Abstract — Our goal is to understand and document the process of designing and fabricating silicon photonic devices from scratch as new designers. Throughout the design process, we study the Mach-Zehnder Interferometer (MZI) and specifically a length-mismatched polymer-modulator MZI which we then fabricate in-house. This is an example of how quickly one can get accustomed to the design process and with access to tooling and training, can produce electro-optic (EO) modulators achieving a 10% π -phase shift in first-draft designs .

I. INTRODUCTION

As an introductory undergraduate course at the University of British Columbia, ELEC 463: Micro/Nanofabrication Laboratory provides students with little or no background in the emerging field of silicon photonics or VLSI fabrication the opportunity to learn the theory of a fundamental device, then fabricate it in a small-scale lab with access to cutting edge equipment and processes.

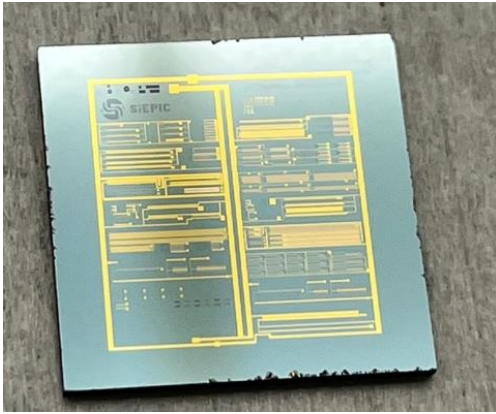


Figure 1: Completed fabricated silicon-photonics chip produced in the Steward Blusson Quantum Matter Institute laboratory with classmates in ELEC463.

This is an opportunity to study polymer based electro-optic effect interferometer modulators using state of the art chemistry with the potential to achieve over 100gbits/s modulation [1]. Not only is the data transfer rate attractive, but EO modulators are an energy-efficient solution with low propagation losses, and are soon likely to be integrated in various datacenters that currently spend significant portions of their energy budget on heating and cooling [2]

We first model a basic Mach-Zehnder Interferometer (MZI) and study the effects of length mismatch in the interferometer arms. This is a static example of how modulating works. As we study the fundamental physics of the devices to fabricate, we also study the workings and physics of the manufacturing tooling and processes to

understand how manufacturing variations affect how the device is fabricated and how it differs from what we design.

We then actually manufacture the devices we design in CAD, going through the design process from a wafer of Silicon on Insulator through lithography and metallization in the laboratory facilities located on-campus in the Stewart Blusson Quantum Matter Institute (QMI). Here we not only manufacture but validate our designs and empirically measure and see our working designs outside of computer modelling and simulation using the Laboratory's suite of optical signal processing equipment.

Our major intentions for this project are to measure our devices nominally throughout the manufacturing process to understand said process variations, and to validate our interferometer process by successfully recording expected effects when we modulate our interferometers. Validating our small-scale process also legitimizes the ability to rapidly prototype silicon photonic circuits and optimize designs over multiple processes in time frames shorter than typical large scale fabs.

II. MODELLING AND THEORY

A. Mach-Zehnder Interferometer

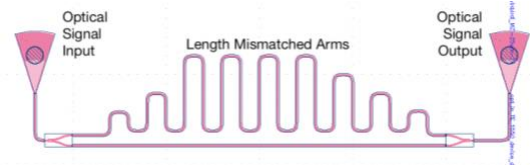


Figure 2: Example of Length Mismatched MZI designed with the SiEPIC-EBeam-PDK

A Mach-Zehnder Interferometer operates the principle of a traveling pulse of light in a waveguide being split and recombined. Below is the transfer function (1) derived by Dr. Chrostowski [3], and the lossless ($\alpha = 0$) case below (2):

$$H(\lambda) = \frac{I_O}{I_I} = \frac{1}{4} |e^{-i\beta(\lambda)L_1} + e^{-i\beta(\lambda)L_2}|^2, \quad (1)$$

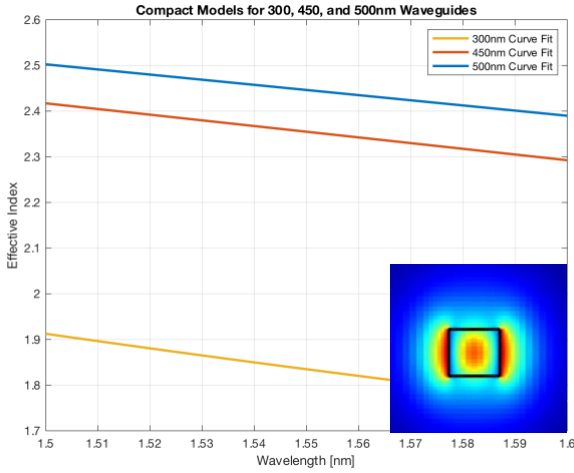
$$\frac{I_O}{I_I}_{lossless} = \frac{1}{2} (1 + \cos(\beta_1 L_1 - \beta_2 L_2)) \quad (2)$$

Where the term β is the complex propagation constant including the propagation loss that is dependent on the n_{eff} of the waveguide material.

$$\beta = \frac{2\pi}{\lambda} \left(n_{eff} + \frac{\delta n_{eff}}{\delta V} V \right) - i \frac{\alpha}{2} \lambda, \quad (3)$$

The term n_{eff} is the comprehensive index that considers the mode solution to the waveguide. It considers geometry of the waveguide, the impact of varying the wavelength of our input sweep, and polarization of the signal. For this investigation we only focus on the first quasi-TE mode of the waveguide. We use a 2nd order Taylor Series expansion for simplicity, and we see how it changes for example with waveguide width.

$$n_{eff} = n_1 + n_2(\lambda - \lambda_0) + n_3(\lambda - \lambda_0)^2 \quad (4)$$



300nm	$n_{eff} = 1.8348 - 1.4801(\lambda - 1.55) - 1.4423(\lambda - 1.55)^2$
450nm	$n_{eff} = 2.3548 - 1.2457(\lambda - 1.55) - 0.0355(\lambda - 1.55)^2$
500nm	$n_{eff} = 2.4462 - 1.1262(\lambda - 1.55) - 0.0405(\lambda - 1.55)^2$

Figure 3: Different effective indices for varied waveguide widths and wavelength sweep, with respective Waveguide Compact Models below. Compact models are derived from Palik using Lumerical MODE with instruction from Dr. Chrostowski [3]. Inset: 220nm by 300nm waveguide signal intensity for TE polarized wave simulated in Lumerical MODE.

In an interferometer with identical arms, we get the nominal loss for all wavelengths of optical signal we input. In cases where we have non-identical beta terms or lengths, we observe a sinusoidal pattern that converted into a logarithmic gain looks like as, as well as an example of how the spectrum shifts is below.

We measure the distance between subsequent maxima or minima known as our interferometer's Free Spectral Range. It can be measured but also calculated as a function of our device's group index as derived in [4]:

$$FSR = \Delta\lambda = \frac{\lambda^2}{\Delta L \left(n - \lambda \frac{dn}{d\lambda} \right)} = \frac{\lambda^2}{\Delta L n_g} \quad (5)$$

The commonly used figure of merit is to find the amount of modulation required to obtain a π -phase shift in spectrum which is equivalent to $1/2$ of the FSR distance at the 1550nm wavelength.

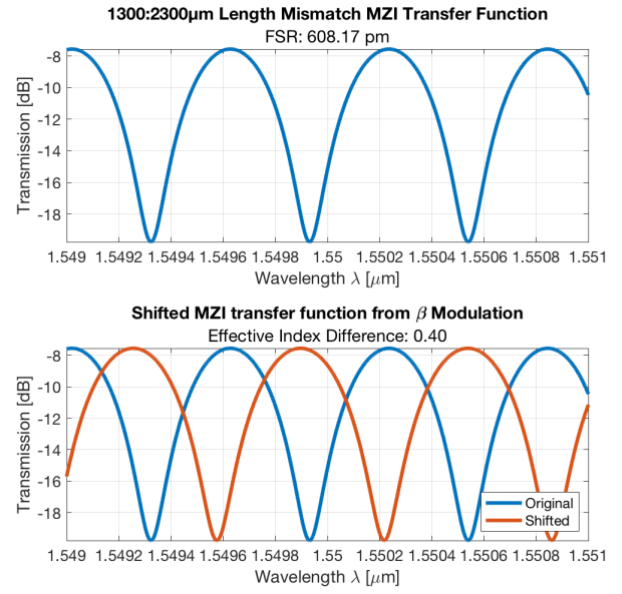


Figure 4: Example of sinusoidal gain in decibels for (top) 1000 μm length mismatched MZI, and (bottom) estimated shift of spectrum for an example change in effective index coefficients of waveguide compact model. Both use a 10pm wavelength sweep resolution about the 1550nm wavelength.

B. Pockels Effect:

To modulate this interferometer, we can use the Pockels Effect on the material surrounding the waveguide to vary the effective index of the waveguide. The relationship of the changing index of refraction of the polymer is derived [5]:

$$\Delta n_{eop} = -\frac{1}{2} n_{eop}^3 r_{33} E = \frac{1}{n_{eop}} \chi^{(2)} E, \quad (6)$$

Where n_{eop} is the refractive index of the polymer and the r_{33} is the electro-optic coefficient, representing how well the chromophores within the polymer are aligned based on polling. We are using a 2:1 ratio of HLD1:HLD2 and can expect the following values given a polling voltage:

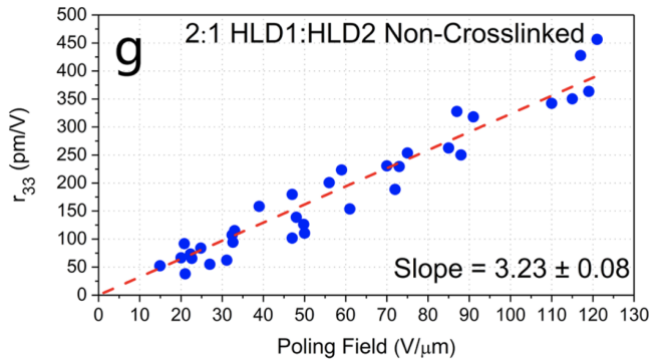


Figure 5: Fitted relationship between Electro-optic Coefficient, r_{33} , and Poling Field by Xu et al [1].

During modulation, we assume that the change in our effective index is proportionally related to our change in refractive index of polymer by:

$$\Delta n_{eff} = \Gamma \Delta n_{eop}, \quad (7)$$

Where Γ , the Confinement Factor, is the fraction of signal travelling within our polymer on the exterior of the waveguide, illustrated in Figure 3. To obtain a π -phase shift for a given modulation voltage, we would like to find:

$$\Delta\beta L = \pi$$

$$\pi = \frac{2\pi}{\lambda} \Gamma \left(\frac{1}{2} \frac{n_{eop}^3 r_{33}}{d} \right) V_\pi \cdot L$$

$$V_\pi = \frac{\lambda d}{\Gamma n_{eop}^3 r_{33} L} \quad (8)$$

Where we can also write our estimated $V_\pi L$ per device.

III. DESIGN

A. Design objective

For this course, we are attempting to utilize the polymer-optic effect to create a working modulator for the first time as new designers. Our *Figure of Merit* is to design an interferometer that optimizes the Pockels effect and although we do not know the yield for this new process, we'd like to maximize the effect if we were to obtain a functioning device. This can prove to us the benefit of the polymer-optic effect over one manufacturing cycle we undergo during a 12-week university semester.

B. Design Methodology

As new designers, we adopted a simple design flow of translating our basic MZI theory into a layout with only the idea to optimize the Pockels effect. Knowing that effect increases with a longer interaction period [3], we designed the effected arms to be as lengthy as possible. Also knowing the Pockels effect creates a small perturbation in the effective index, we want to be able to see the effect as obviously as possible [3]. For this reason, we choose an imbalanced MZI layout with a very small FSR to view any excitations we may see on a similar scale.

C. Design of Experiment

Below in Table 1 we list 6 devices to fabricate and run our polymer-optic effect experiment on. To add further redundancy of having visible polymer-optic effects, we added a 350nm wide waveguide configuration. In Figure 8, it's visible that with a smaller width waveguide there is a larger portion of stable optical signal existing outside the waveguide in the surrounding material. When our polymer's effective index is modulated, the more signal we have interacting with the polymer would affect our response.

Listed in Table 3 are our Test Structures that characterize noise that is generated in our signal from the grating couplers. It was specified to keep these as close as possible to our devices to ensure they accurately represent the losses we see when we measure our devices.

We can estimate our $V_\pi L$ for our devices with the given constant design choices in Figure 7.

Design of Polymer-Optic MZI Devices				
Design #		Wave Guide Width	ΔL	Max L
Short	1	350 nm	1000 μm	2312 μm
	2	500 nm	1000 μm	2332 μm
Long	3	350 nm	1500 μm	15012 μm
	4	350 nm	2200 μm	15712 μm
	5	500 nm	2200 μm	15732 μm
Big	6	350 nm	3000 μm	~30000 μm

Table 1: Variations of Polymer-Optic Modulators to fabricate and Test. All are in unbalanced MZI configurations with length mismatch of ΔL and longer length arm of Max L. They are to be injected with 1550nm wavelength TE optical signal.

Predicted Device Performance				
Design #		Expected FSR	Expected V_π	Expected $V_\pi L$
Short	1	608.2pm	630V	126cm
	2	608.2pm	630V	126cm
Long	3	399.2pm	84V	126cm
	4	399.2pm	84V	126cm
	5	399.2pm	84V	126cm
Big	6	198.0pm	42V	126cm

Table 2: Calculated Performance of Devices. V_π 's calculated using Python Script provided in Appendix, and FSR from MATLAB code also in Appendix.

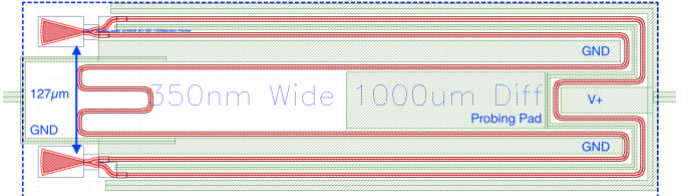


Figure 6: Short-1 Device with labelled electrical connections. Both arms of the interferometer are polled, but only from the Probing Terminal to Ground is modulated and affected. This Design can easily create variants with different lengths and mismatches.

Test Measurement Structures		
Design #	Wave Guide Width	Measurement
7	350 nm	Decoupling
8	500 nm	Decoupling
9	500 nm	Decoupling with Y-Branch

Table 3: Test Structures on or nearby devices under test used for determining insertion loss and to validate any noise added by fiber array and grating coupler during measurement.

Polling Distance	25 μm
Modulating Distance	10 μm
Polling Voltage	200V
Expected r_{33} value	20pm/V @ 8V/ μm Field

Figure 7: Parameters kept constant between designs for this manufacturing run but can be changed for future designs to alter device performance.

D. Manufacturing variability

As noted in Figure 8 we can see the potential effect of variations on our signal. One way to note potential outcomes and to better understand our fabricated device is to corner analysis and Monte Carlo simulations to our designs which we can then compare with our simulations. With this comparison, we can better estimate dimensions of our devices that we cannot accurately measure, such as the actual width of our devices, without destructive techniques.

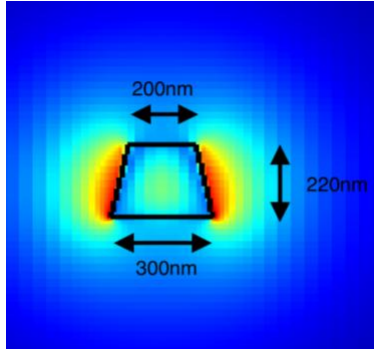


Figure 8: Left: Intensity of 1550nm signal in first TE Mode injected into 300nm wide by 220nm tall Si on SiO₂ waveguide, showing amount of signal outside Silicon waveguide in surrounding material (air) useful for polymer-optic effect. Right: Changes of confinement factor when manufacturing variation such as sloped walls occurs and how this variation can be an advantage with polymer-optic effect.

E. Mask Layout

To manufacture these devices, we first design the mask layout we will use for our specified process using the SiEPICfab EBeam ZEP PDK [6] in the KLayout GDS Layout Tool. To achieve best yield, we followed the following design rules provided [7] and as specified in the appendix. An important design rule we followed was labelling each device's input signal grating coupler, saving coordinates which we use in automated measurement.

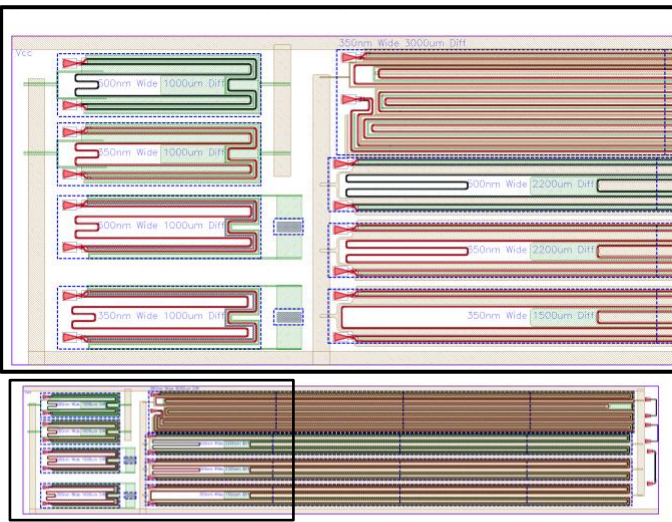


Figure 9: Full Mask Layout with zoomed area of interest above. Six Polymer-Modulators connected to global Polling Electrodes (top and bottommost metals) and two backup Thermo-Optic Effect Modulators (bottom-left) along with three decoupling test structures (right). Designs optimized for long lengths and small FSRs with variation in waveguide width.

A major rule involved keeping our electrical probing pads 500 μ m away from our correctly oriented grating couplers to allow us to measure and modulate our devices at the same time. Other rules involved preventative design to avoid overlap and bleeding between areas of fine geometry that have been learned in previous process yields [3]. A large design constraint was to utilize global polling pads to poll the entire chip rather than individual devices.

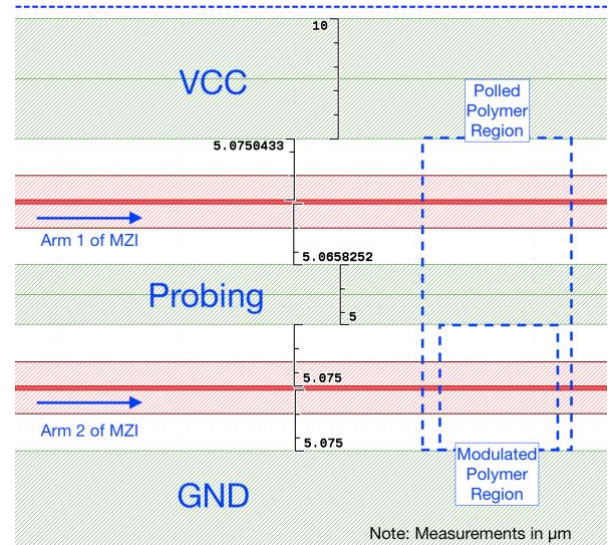


Figure 10: Enlarged view of Short-1 MZI (350 Wide, 1000 Δ L). Annotations denote distances between metal and Silicon features, regions of polling and modulation, and metal connections. Polling occurs in the electric field between VCC and GND, and the modulation only affects polymer between Probing and GND metal connections. All measurements are in micro-meters.

IV. MANUFACTURING AND TEST PROCEDURE

A. Fabrication

To manufacture our chips, we had our Teaching Assistant (TA) Donald Witt who was trained for the Clean Room Lab equipment prepare, etch, and clean our chips. It is very important to cut multiple chips as we use some to set-up processes as well have redundancy in the event of process variations and defects. We marked the underside of the 6 chips that we began our process with and stored in a clean gel pack.

Our manufacturing steps are outlined in Table 3:

Stage	Steps	Figure
Prep	Dicing of Wafer Cleaning of Wafer	Figure 12
Silicon Etching	EB Resist Spin + Baking BEAMER Electron Beam Lithography EB Resist Development Plasma Etch Post-Etch Cleaning	Figure 12
Validation	Microscope Imaging Automated Testing	-
Metal-ization	PhotoResist Spin + Bake Photolithography PhotoResist Development	Figure 14

	Metal Evaporation/Deposition Lift-off	
Validation	Microscope Imaging Automated Testing	-
Adding Polymer	Plasma Etch Cleaning Polymer Mixing Polymer spinning	Figure 15
Polling	Polling of Polymer	-
Data Collection	Microscope Imaging Manual Probing Testing	-

Table 4: Overview of Fabrication Steps followed.

1) Dicing of Wafer

We begin with procuring a Silicon on Insulator (SOI) wafer from our supplier [?]. Using the DISCO DAD3240 Dicing Saw [8] we can cut the size of wafer we need, then clean our silicon surface using acetone and isopropyl.

2) Electron Beam Resist:

We are doing a **Negative EB-Resist** using the ZEP Process. As in Figure 11, this allows us to cost- and time-effectively etch away portions of Silicon on the top layer of our SOI wafer *around* our devices instead of over the entire chip which is unique for our ZEP Process.

With one of our diced chips as a test chip, we place it on 180°C hot plate for 30min while cleaning the 200mm Headway Spinner with acetone and drying with N₂ gas [9]. After timer expires apply Zep520A Resist covering 60% of the wafer. Spin using ramped program as in Appendix on the 200mm Headway Spinner. Immediately return to hot-plate and bake at 180°C for 2min. Using the FILMETRIX F20 Thin Film thickness measurement system [10] we can measure the amount of resist we apply ensuring we achieve 530 to 560nm of resist [9]. We can take this measurement in several locations on the test chip to verify we have an even spread. If needed we can clean, adjust our steps, and re-apply until we verify our process and proceed to apply resist to the other chips.

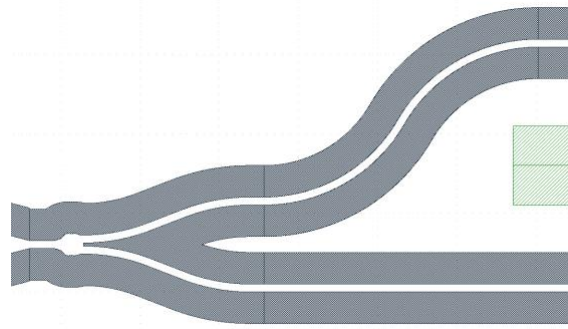


Figure 11: ZEP-EBeam-Process where white is Silicon to keep and grey is Silicon to be etched. The surrounding Silicon has no effect on our devices performance wise and is usually etched away when using a Photolithography process.

3) Electron Beam Lithography

Prior to lithography, we used the BEAMER Software [11] to map out which parts of our designs would have the highest

Electron Beam current, focus, and time of exposure onto the EBL-Resist. For rough edges we can go faster with less focus and a higher current but on our waveguide edges, where we want smooth sidewalls, we increase the focus and ensure that there is no scattering of our beam. This allows the resist on top of our waveguide to be as untouched as possible by the electron beam leaving a very distinct difference from etched and non-etched areas after the etching process.

The UBC SiEPIC Lab has access to a Jeol JBX-8100FS Electron Beam Lithography System [12] that Donald will run to weaken the EBL-resist overtop of our etch regions.

Before applying the various dosages of electron beam to our chip that we calculated using BEAMER, we spend multiple steps aligning and calibrating the machine to our chip's height and area to ensure the beam is in focus on each part of our chip following our Runsheet [13, 14]. Due to material variations in our SOI wafer, the machine creates a heightmap of our chip, so in areas that are taller/shorter the beam can be focussed appropriately to properly react with the EBL-Resists that are at different heights.



Figure 12: Process Cross Sections per procedure that were used to develop a waveguide using the ZEP-E-Beam-Process using the on-site tooling and equipment in Dr. Chrostowski's lab.

4) Resist Development

Shortly after lithography, Donald developed the chips in ZED-N50 and washed with IPA on the isothermal plate at 20°C [15]. We do this in a very controlled process where we rinsed out the beakers with the chemicals to prevent any contaminants from entering the reaction. We place the chip in the ZED-N50 for 1 minute slowly agitating vertically before precisely removing at the 57 second mark and immersing in the IPA solution at the 60 second mark.

5) Plasma Etch and Residue Removal:

We have access to an Oxford Instruments PlasmaPro 100 Cobra ICP RIE Etching machine. This machine allows us to do a highly selective dry etching in a plasma environment, as well as highly directional physical etching using Reactive Ion Etching all in the same process.

Our first step in the etching process is cleaning the etching chamber. This clears any residue left by previous processes that may introduce impurities into our process. Now with a clean etching environment, we run our etching program on an empty wafer **without** our chip present. This allows the

environment of our first etch to be as like the environments of the etches afterwards. In our lab we have empirically found that running 5 etches serially is our general limit for keeping the etching chamber consistent.

After setting our environment we attach our chips onto the empty holding wafer with vacuum grease and proceed with the etching program. Our etching program runs with the following parameters:

Parameter	Value	Units
Chamber Pressure	10	[mTorr]
SF ₆ Gas Flow	25	[sccm]
C ₄ H ₈ Gas Flow	35	[sccm]
ICP Power	600	[W]
Table HF Power	30	[W]

Figure 13: Machine settings for PlasmaPro 100 Cobra ICP RIE Etching Machine used for our ZEP-EBeam-Process to dry etch our silicon and electron beam resist.

We turn the gasses sulfur hexafluoride, SF₆, and isobutylene, C₄H₆, into plasma by fluctuating a magnetic field from the inductor in the chamber to induce electric fields that supply energy to the atoms [16]. This leads to the atoms in the gas to undergo most commonly the dissociation and ionization chemical reactions that create species that participate and enhance the etching process [17].

Once etched, we use chemicals Remover PG along with EKC265 to remove any leftover debris after etching. These are done at very specific temperatures and times and before doing we must remove any remaining vacuum grease from the backside of the chip with ethyl acetate and clean our tools, specifically our custom-designed Teflon sample holder, with Acetone, IPA, and N₂ gas specifically in that order to prevent leftover residue. [18]

We use one beaker of Remover PG on the stirring hotplate at 80°C, one beaker of EKC265 on another hotplate also at 80°C, another beaker of PG Remover at room temperature, and 5x beakers of IPA. [18]

We do 15 minutes in the hot Remover PG, then place in the room-temperature Remover PG for 5 minutes. After this timer, we dunk rinse in the two IPA beakers one at a time before placing in our EKC265 for 30 minutes. After this we do the same dunk rinsing with 3 beakers of IPA to remove any leftover chemical. [18]

6) Photore sist Spinning, Photolithography, and Development

To add our probing and polling metals to our chip, we apply a similar process but use photolithography on our resist rather than electron beam lithography to take advantage of its fast write-time that blankets the whole chip instead of serially writing the layout.

Before spinning our photore sist, we very quickly clean our chip in a O₂ Plasma Etch for 5-minutes in the small dry etcher in the lab [19]. As that finishes we clean and program the spinner then we first apply LOR2A, baking for 5 minutes at 200°C on a hotplate. After baking, we use our second photore sist and program our second spinner program to apply the AZ5214 photore sist, which we then bake for 1 minute at 98°C. We can use the FILMETRIX F20 Thin Film

Measurement System to obtain the height of resist we apply which needs to be significantly higher than 105nm to ensure proper lift-off.

After baking we transfer to a carrier wafer and place our chip in the MLA-150 Maskless Lithography System [20]. After lithography, we develop in MIF300 for 45 seconds, quickly transferring and rinsing for 10 seconds in de-ionized water, completing our photoresist mask.

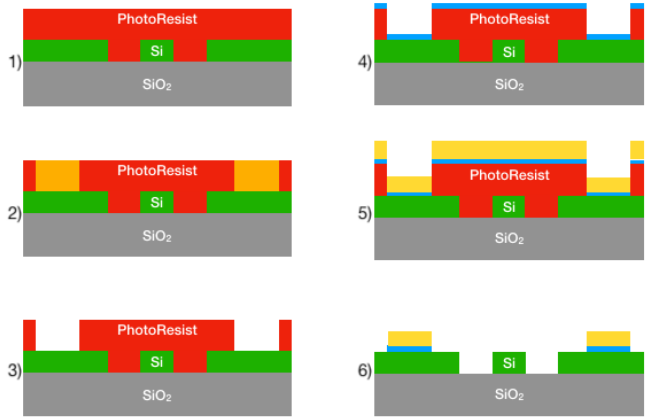


Figure 14: Metallization Process, starting with high amount of (1) photoresist, (2) lithography, (3) development, (4) Titanium Evaporation Deposition, (5) Gold Evaporation Deposition, (6) and Lift-off Etching. All processes were conducted in SBQMI Clean Room (not to scale).

7) Metal Evaporation

To deposit metal on our chip, we use the process of metal evaporation using the AJA Hybrid Evaporator System to chemically bond our metal to our silicon [21]. After securing our chip with Kapton tape, we first deposit 5nm of Titanium, then 100nm of Gold. If you're reading this, make sure you take the tape as a souvenir as Bruce did and it was very cool to see him have a piece of tape covered in <1mm of gold. Lukas also mentioned he had to go into the back room of a jewelry store to purchase the gold nugget that we evaporated [3].

8) Metal Lift-off

Using Remover 1165 [19], we leave the chip overnight in a beaker for the resist under the metal to break apart and lift-off. We did require some ultrasonication the day after to agitate some of the metal that did not lift off initially. This is a step where yield can be affected as due to non-removed metal, metals joining from ineffective mask distance between metals, and too much metal removed during ultrasonication.

9) Polymer Application

Our last step in manufacturing is spreading our polymer. We do this by bringing our HLD1 and HLD2 mixtures to room temperature from refrigerated storage and mixing a 2:1 weight ratio of HLD1:HLD2 which we then add TCE solvent to create a 9% weight liquid solution [22]. For thinner films a 5% weight solution can be used. We do not have the ability to predict our variables of interest from this manufacturing stage but attempt to cover our chip completely ensuring that the space between our metal and waveguide is filled.

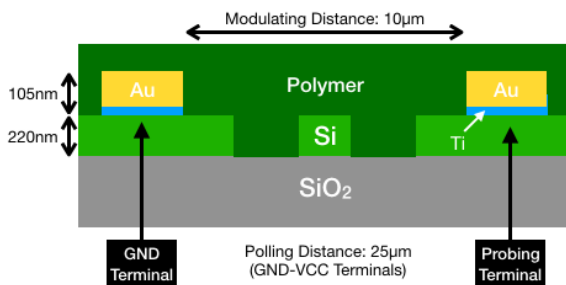


Figure 15: Completed Fabrication Cross Sectional schematic of EO Modulator, viewing modulated arm of MZI (not to scale).

B. Measurement Procedure

For the following, please contact the author of this paper or fellow classmates until updated later.

1) Fibre Array and Automated Testing

Using our laboratory's automated testing system, we need to first orient our chip on our stage and configure our constant temperature monitoring. Our stage consists of a mounted microscope and ThorLabs linear XYZ motion controlling system. To ensure translation between the stage and chip are aligned, we need to rotate our chip along each axis for proper orientation. It is important to verify and correct any height differences around the chip to prevent potential crashing of the chip and fibre array which we bring towards our microscope FOV. Once properly oriented, we can open the stage's vacuum connection to hold our chip down. Once here, we can activate our temperature control to maintain our chip's temperature at a steady room temperature void of any fluctuations that can vary measurement results.

With an oriented stage, we can now run our lab's custom program to map our GDS layout file to our physical chip using alignment markers that we included in our masks during design. Once mapped we can select which device we would like to measure, and our stage will automatically move to center that location.

Using the laser output connected to our calibrated fibre array, we can input an optical signal sweep and measure its response. We note that signals measured under -50dB were considered noise and aimed to reach signal strengths of -30dB, a value determined by previous propagation loss studies [23].

We conduct automated testing during the manufacturing process to verify yield at the stages before and after metallization. It is noted that testing after adding polymer requires scratching off the polymer at probing pads to achieve electrical connection.

2) Polling:

We first fix a portable microscope stage containing a heating element inside a chemical hood, then setup electrical probes, scratching off the polymer located above them. We verify are connected to our global polling pads, then begin the process of polling. We use reference to the manufacturer provided polling instructions [22] but due to equipment issues we could only poll to a maximum temperature of 115°C [23]. We hold intermediate temperatures for 10min and ramp up at 10°C/min from room temperature to our maximum of 115°C.

3) Polymer Modulation

As we were unable to poll our devices, this will be updated at a later date when possible.

V. ANALYSIS

A. Devices Under Study

Note: During measurement of other devices on the chip, a short had suspected to occur which had raised the temperature of the chip far above its temperature to de-align polymers.

Using the laboratory optical signal tools, we can sweep input wavelength and find our results.

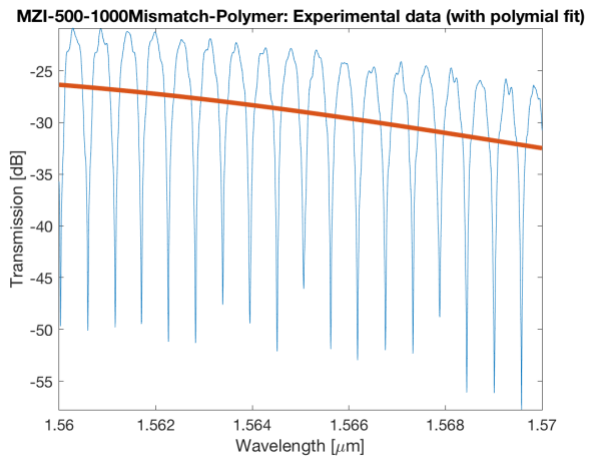


Figure 16: Raw Experimental Data from generated from 100pm resolution wavelength sweep for one device. Red line is a baseline curve fit of the general trend the data is tending towards to remove for correction.

We can see our interferometer's transfer function in the data but need to remove the offset and any noise. We can do this by method of linear interpolation in MATLAB. We attempt to curve fit this data but have some difficulty with our datasets due to measuring resolution. Once curve fitted we can extract various parameters of our device and work backwards to discover any variations in dimensions and performance caused by fabrication.

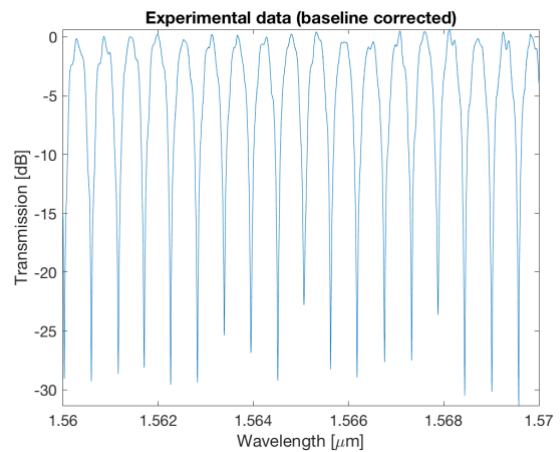


Figure 17: Experimental MZI Data modified using baseline-correction to better curve-fit and provide data without noise of grating couplers or insertion loss.

B. Example of Measured Devices:

We will use the data of our classmate, Felix Klose, to show the analysis of a device that was able to be measured.

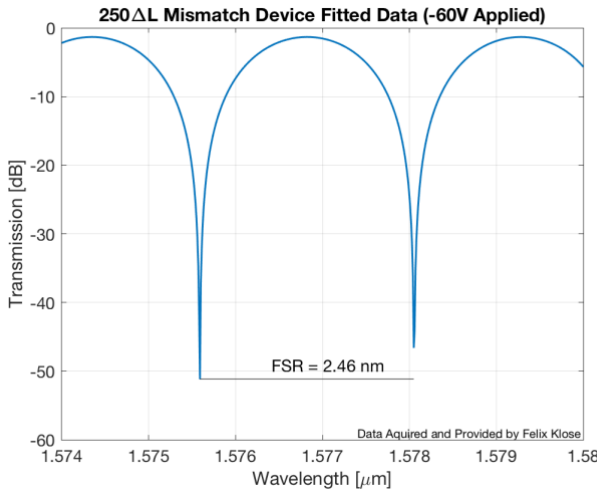


Figure 18: Fitted MZI Data for Klose device measured at SBQMI. FSR is extracted using MATLAB 'findpeaks' function.

By our relationship between FSR and group index in equation (5), we can determine our group index to be approximately 3.8594 at an inferred 1550nm wavelength, which we can also do from our curve fit:

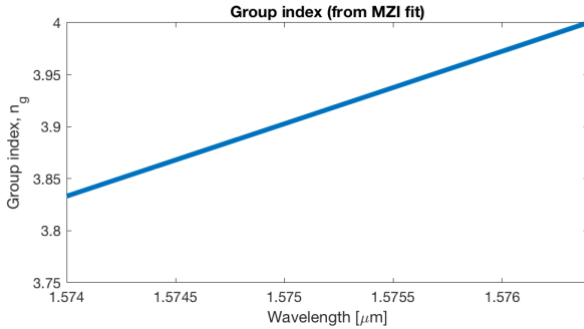


Table 5: Experimental Analysis of Group Index from fit of raw data.

During curve fitting we produce our model's effective index which despite being not the same device as we have designed, we can still compare to validate coefficients generated in simulation. They mean very little as the models were generated about different reference lambdas.

Klose Device: Effective Index Parameters obtained during Curve-Fitting about 1.5770μm (width = 500nm, 0V applied)			
n_1	n_2	n_3	α [dB loss/cm]
2.3492	-1.0732	-22.0950	9.7785e-9

Table 6: Effective Index coefficients for Taylor Expansion Polynomial and loss coefficient generated from curve fitting process.

Birdi Device: Effective Index Parameters Simulated from untested Design about 1.550μm (width = 500nm)			
n_1	n_2	n_3	α [dB loss/cm]
2.4462	-1.1262	-0.04505	0.001

Table 7: Simulated Effective Index Parameters from designed device. This was generated using Lumerical MODE

C. Shifted Spectrum:

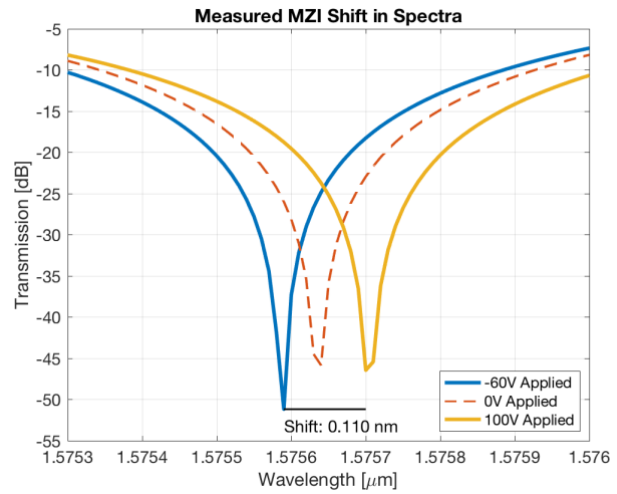


Figure 19: Shifted Spectrum of MZI when applying -60V and 100V to modulation contact pads after poling step. This is limited by the method of how we fit our noisy data and needs to be verified as reproducible using other methods before being considered fully legitimate.

We see a 0.110nm shift in our 2.49nm, approximately 4.47% of our FSR, and **8.94% of our ½ FSR π-phase shift distance**.

Using the parameters we generated in curve fitting, we can compare the effective indices' Taylor Expansions to investigate how the applied voltage from -60V to +100V shifted the effective index:

Klose Device Effective Index				
Applied Voltage	n_1	n_2	n_3	n_{eff} at 1.5755μm
-60V	2.349079	-1.09971	-4.61864	2.3507
+100V	2.349366	-1.15694	-39.8388	2.3510

Table 8: Effective Indices for Applied Voltages of measured Device, showing a Δn_{eff} of approximately 0.0003.

We recap Equation 4 for reference:

$$n_{eff} = n_1 + n_2(\lambda - \lambda_0) + n_3(\lambda - \lambda_0)^2 \quad (4)$$

And note that despite the shift in spectra we do not observe a large change in effective index. At our reference wavelength, taken as the average from our data, 1.5770μm, we calculate the effective index at 1.5755μm where our interference pattern occurs to find only a 0.0003 difference in effective index. We can use this to determine experimentally how well our r_{33} value was manufactured using the relationship in Equations (6) and (7) using $\Gamma = 0.15$, $n_{eop} = 1.6$, and $V = 160V$ with $d = 10\mu m$:

$$r_{33} = -2 \left(\frac{\Delta n_{eff}}{\Gamma} \right) \frac{d}{n_{eop}^3 V} = 61.03 \text{ pm/V} > 20 \text{ pm/V} \quad (9)$$

This value of r_{33} is much higher than our anticipated value of 20pm/V that we determined from our Poling Voltage and Poling Electrode distance. investigations. A 3x increase in r_{33} does lower our necessary V_{π} by a factor of three, so if true this is very good to see.

It is important to mention with further modelling data we can accurately compare what we have fabricated to what we design. Using primarily our effective index, we can apply a corner analysis and simulate the effective index at each variation of dimensions as in the figure below:

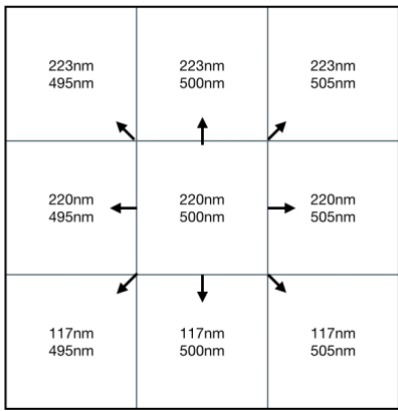


Figure 20: Two-Dimensional Corner Analysis of Height and Width of manufactured Waveguide. We can compare our fabricated device with the range of simulated effective indices to gain insight on what device dimensions were fabricated.

VI. DISCUSSION

As a first time designing and utilizing this process, there was and still is much to learn. A key factor in analysis of data was using a finer resolution wavelength sweep for the designed devices to obtain data usable for curve-fitting. In cases of larger FSRs where I did not think it was an issue, I still found it caused some difficulty in curve-fitting:

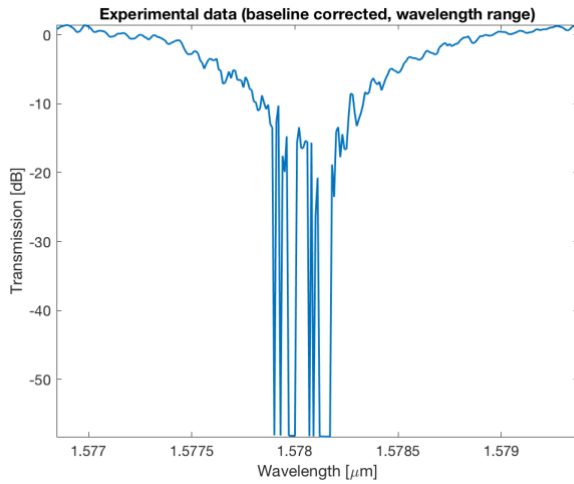


Figure 21: Example of messy experimental data. Using finer resolution wavelength sweeps can possible aid this to allow better curve fitting.

Another note is the process of analysis and the important role of automation within it. A single device takes time to characterize; but when observing trends in variation and yield, the methods used to analyse must be robust that it is simple to not only replicate analysis but also compare with other devices. Creating programs for analysis required this not as an

afterthought to easily compare results from one device study to another.

Seeing a significant shift in our modulated device was a very important figure of merit in that the device worked with our first-time process. We did not achieve our intended figure of merit of a π -phase shift but can now design with more confidence and better choices to achieve this in the future. This is very possible as we've outlined designs that have a $V\pi$ that have capability to apply.

From applying the relationship in Equation (9), we can determine from our r_{33} value that we were able to poll our device substantially better than we predicted. I strongly believe that this needs to be verified reproducible in further investigations as much of our data needed to be recorded at a higher resolution to help us better fit our data.

Our results of our study unfortunately do not represent the devices designed, but it was a valuable exercise to analyze results of measured devices and validate a phase-shift. With this information, I would like to test the devices I've designed in the future to validate the impact of smaller waveguide widths and affected distance.

During design, we did not know the full impacts of some of our decisions. Some changes in future designs include applying better strategies for poling. The concept of group poling did prevent us from achieving tight poling distances but can be improved using newer technologies such as Photonic Wire Bonding to jump over waveguides or by adding more layers to the chip for metal routing to solve this topological problem.

A significant solution discussed in class [3] as well as in [24] is to use slotted-strip-waveguides to carry the electric field closer to the region of poling. Liu et al. also discuss placing the *metal overtop of the polymer* which is a strong method provided sufficient adhesion [24]. A proposed solution that can be manufactured is by trying the same idea with the design below. This can double our r_{33} values by shortening the distance of poling by a factor of two.

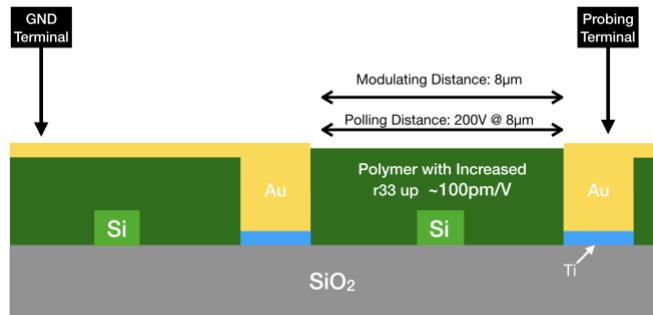


Figure 22: Revised Design to increase r_{33} by decreasing poling distance from 25 μ m to modulating distance of 8 μ m. Anticipated r_{33} of 100pm/V from our achieved of 60pm/V. Inspired by Liu et. al. [24]

This is one solution to increase phase shift but requires a new fabrication process to deposit gold atop the polymer. Another solution that does not require different fabrication would be to verify long interaction periods of extremely long branches does not cause significant loss. It is very easy to

create longer designs rather than rework a fabrication process. As we see in Table 2, we can lower $V\pi$ by extending length when our $V\pi L$ determined by fabrication stays constant.

VII. CONCLUSION

As a small scale fab, it is possible to manufacture devices in low volumes, but the analysis of manufactured devices and chips still require the same effort as done in large scale manufacturing. Given our freshness to the process and availability of tools, it is possible to perform analysis as a small scale fab, but experience is an invaluable asset that can develop workflows to gain better insight and analysis of devices.

Working in a classroom setting was extremely useful as collaboration with peers during lecture hours exposed many new perspectives, as well as the variety of designs and routes of analysis showed myself newer and better ways to design and conduct analysis.

ACKNOWLEDGEMENT

Thank you to Iman Taghavi who aided in performing measurements, Donald Witt who aided in the fabrication, CMC Microsystems for providing the design tools, Dr. Lukas Chrostowski for the theory and insight during lecture. I would also like to thank my lab-mates pictured below who I worked with this semester for their collective help and questioning to further understand this design and fabrication process.



Figure 23: ELEC463 Tuesday Laboratory Section after completing fabrication

REFERENCES

- [1] F. L. D. L. E. L. E. J. Y. d. C. K. C. B. H. R. a. L. R. D. Huajun Xu, "Ultrahigh Electro-Optic Coefficients, High Index of Refraction, and Long-Term Stability from Diels–Alder Cross-Linkable Binary Molecular Glasses," *Chemistry of Materials*, vol. 32, no. 4, pp. 1408–1421, 2020.
- [2] J. H. ., F. Q. A. M. S. T. K. J. O. M.-a. O. H. N. & S. Y. Guo-Wei Lu, "High-temperature-resistant silicon-polymer hybrid modulator operating at up to 200 Gbit s⁻¹ for energy-efficient datacentres and harsh-environment applications," *Nature Communications*, vol. 11, no. 4224, 2020.
- [3] L. Chrostowski, *Classroom Lecture*, Vancouver, BC, 2021.
- [4] L. Chrostowski, "The free spectral range (FSR) of the imbalanced interferometer," [Online]. Available: <https://edx-course-phot1x-chrostowski.s3.amazonaws.com/ng.pdf>. [Accessed September 2020].
- [5] P. Steglich, "Silicon-on-Insulator Slot Waveguides: Theory and Applications in Electro-Optics and Optical Sensing," *IntechOpen*, vol. <http://dx.doi.org/10.5772/intechopen.75539>, no. Available from: <https://www.intechopen.com/chapters/60221>, p. 201, 2018.
- [6] L. Chrostowski, "SiEPICfab-EBeam-ZEP-PDK," Github, [Online]. Available: <https://github.com/SiEPIC/SiEPICfab-EBeam-ZEP-PDK>. [Accessed 20 October 2021].
- [7] L. Chrostowski, "UBC-ELEC463 Repository," Github, [Online]. Available: <https://github.com/SiEPIC/UBC-ELEC463>. [Accessed 20 October 2021].
- [8] SBQMI Advanced Nanofabrication Facility, "DISCO DAD3240 Dicing Saw," UBC, [Online]. Available: <https://www.nanofab.ubc.ca/equipment/other/disco-dad3240-dicing-saw/>. [Accessed November 2021].
- [9] D. Witt, "runsheet_spin.pdf," UBC, [Online]. Available: <https://qdot-nexus.phas.ubc.ca:25683/apps/onlyoffice/s/p6MADWkbJdoLAjp?fileId=141181280>. [Accessed October 2021].
- [10] SBQMI Advanced Nanofabrication Facility, "FILMETRIX F20: Thin film thickness measurement system," UBC, [Online]. Available: <https://www.nanofab.ubc.ca/equipment/analysis/filmetrix-f20-thin-film-thickness-measurement-system/>. [Accessed October 2020].
- [11] GenISys GmbH, "Electron- and Laser-Beam Lithography Software," GenISys GmbH, [Online]. Available: <https://www.genisys-gmbh.com/beamer.html>. [Accessed November 2021].
- [12] SBQMI Advanced Nanofabrication Facility, UBC, [Online]. Available: <https://www.nanofab.ubc.ca/equipment/photolithography/jeol-jbx-810ofs-electron-beam-lithography-system/>. [Accessed November 2021].
- [13] D. Witt, "runsheet_ebl.pdf," UBC, [Online]. Available: <https://qdot-nexus.phas.ubc.ca:25683/apps/onlyoffice/s/p6MADWkbJdoLAjp?fileId=141181249>. [Accessed October 2021].
- [14] D. Witt, "runsheet_ebl_page2.pdf," UBC, [Online]. Available: <https://qdot-nexus.phas.ubc.ca:25683/apps/onlyoffice/s/p6MADWkbJdoLAjp?fileId=141181248>. [Accessed October 2021].
- [15] D. Witt, "runsheet_development.pdf," UBC, [Online]. Available: <https://qdot-nexus.phas.ubc.ca:25683/apps/onlyoffice/s/p6MADWkbJdoLAjp?fileId=141181247>. [Accessed October 2021].
- [16] Corial, "Inductively Coupled Plasma – Reactive Ion Etching (ICP-RIE)," Corial, [Online]. Available: <https://corial.plasmatherm.com/en/technologies/icp-rie-inductively-coupled-plasma-reactive-ion-etching>. [Accessed 21 10 2021].
- [17] D. L. Chrostowski, "ELEC 463 Etching Lecture Notes," in *Micro/Nanofabrication and Instrumentation Laboratory*, Vancouver, 2021, pp. 12-14.
- [18] D. Witt, "runsheet_finalclean," UBC, [Online]. Available: <https://qdot-nexus.phas.ubc.ca:25683/apps/onlyoffice/s/p6MADWkbJdoLAjp?fileId=141226574>. [Accessed October 2021].
- [19] D. Witt, "runsheet_metal_liftoff.pdf," UBC, [Online]. Available: <https://qdot-nexus.phas.ubc.ca:25683/apps/onlyoffice/s/p6MADWkbJdoLAjp?fileId=141314476>. [Accessed November 2021].
- [20] SBQMI Advanced Nanofabrication Facility, "Heidelberg MLA-150 Maskless Lithography System," UBC, [Online]. Available: <https://www.nanofab.ubc.ca/equipment/photolithography/heidelberg-mla-150-maskless-lithography-system/>. [Accessed November 2021].
- [21] SBQMI Advanced Nanofabrication Facility, "AJA Hybrid Evaporator System," UBC, [Online]. Available: <https://www.nanofab.ubc.ca/equipment/thin-film-deposition/aja-hybrid-evaporator/>. [Accessed November 2021].
- [22] Nonlinear Materials Corporation, "HLD1/HLD2 Recommended Handling, Solvent Casting, and Poling Please Read BEFORE Using," October 2020. [Online]. Available: https://cdn-uploads.piazza.com/paste/k56328ij3g370x/47e30dec473180353fadbe3f6563b85a9446367dfb85913d36563f6c8b23d1b1/HLD_Storage_Handling_Preparation_-_Nonlinear_Materials_-_October_2020.pdf. [Accessed November 2021].
- [23] I. Taghavi, Interviewee, [Interview]. November 2021.
- [24] Jialei Liu, Guangming Xu, Fenggang Liu, Iwan Kityk, Xinhou Liu and Zhen Zhen, "Recent advances in polymer electro-optic modulators," *RSC Advances*, vol. 5, p. 15784, 2015.

VIII. APPENDIX

A. Modelling:

Modulated MZI Equation:

$$\begin{aligned}
 H(\lambda) &= \frac{1}{2}(1 + \cos(\beta_1 L_1 - \beta_2(L_1 + \Delta L))) \\
 &= \frac{1}{2}\left(1 + \cos\left(L_1\left(\beta_1 - \beta_2\left(1 + \frac{\Delta L}{L_1}\right)\right)\right)\right) \\
 &= \frac{1}{2}\left(1 + \cos\left(\frac{L_1 2\pi}{\lambda}\left(n_{eff,1} - (n_{eff,1} + \Delta n_{eff})\left(1 + \frac{\Delta L}{L_1}\right)\right)\right)\right)
 \end{aligned}$$

B. Design Rules for Mask Layout:

1. Use Strip TE 1550nm Waveguide specification
2. Grating Couplers on Left pointing right
3. Electrical Probing Pads minimum 500 μm from Grating Couplers
4. Minimum Feature Sizes:
 - a. Silicon: 100 nm
 - b. Metal: 5 μm
5. Minimum Space between layers:
 - a. Silicon-Silicon: 100 μm
 - b. Metal-Metal: 5 μm
 - c. Metal-Silicon: 4 μm

C. Headway Spinner Ramp Program:

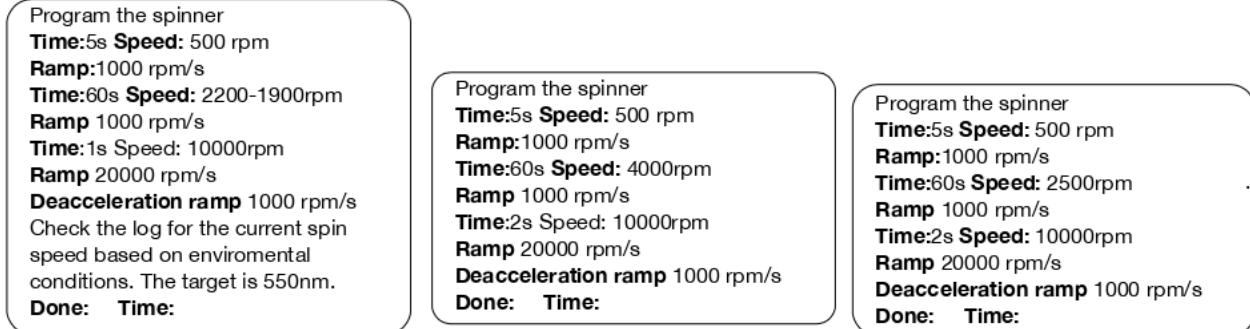


Figure 24: Programming steps when applying (left) Zep520A EBeam Resists to SOI [9], (center) LOR2A PhotoResist [19], and (right)AZ5214 PhotoResist [19].

D. MZI Modelling: Matlab

```

% MZI Length Mismatch Modelling:
% Originally Written by Dr. Chrostowski
% Modulation and FSR Added by Davin Birdi
%
% Running the script will tell you:
% 'X nm FSR for 1000um length mismatch'
%

% the wavelength range of interest.
lambda_min = 1.548; % Units [-μm, microns (1e-6 m)]
lambda_max = 1.552;
% Set wavelength sweep to 10pm [pm, (1e-12 m)]
lambda_step = 1e-6; % wavelength step [microns]
% Typical minimum step for a tunable laser is 1-10 pm.

lambda=lambda_min:lambda_step:lambda_max;

% MZI Length Mismatch:
L1=1300;
L2=2300; % Units [-μm, microns], variable

% Plotting Variables:
lambda_window = [1.549 1.551];
fontsize = 13;

% Define the MZI transfer function using Matlab anonymous functions
% Effective index: Simulate change in WCM
% - as a Taylor expansion around the central wavelength, lambda0
% these are constants from the waveguide model.

lambda0 = 1.55;
n1=2.4; n2=-1; n3=0;
neff1 = @(lambda) ...
    (n1 + n2.* (lambda-lambda0) + n3.* (lambda-lambda0).^2);

% Example of different waveguide model - need to import from Lumerical MODE
n1=2.0; n2=-1.2; n3=0;
neff2 = @(lambda) ...
    (n1 + n2.* (lambda-lambda0) + n3.* (lambda-lambda0).^2);

% Complex propagation constant: beta2 is with modulated polymer
alpha = 1e-3; % propagation loss [micron^-1]; constant
beta1 = @(lambda) ...
    (2*pi*neff1(lambda)./lambda - li*alpha/2*ones(1,length(lambda)) );
beta2 = @(lambda) ...
    (2*pi*neff2(lambda)./lambda - li*alpha/2*ones(1,length(lambda)) );

% MZI transfer function: nominal is using neff1, modulated: neff2
T_MZI_nominal = @(L1, L2, lambda) ...
    ( 0.25* abs(exp(-li*beta1(lambda)*L1)+exp(-li*beta1(lambda)*L2)).^2);

T_MZI_modulated = @(L1, L2, lambda) ...
    ( 0.25* abs(exp(-li*beta1(lambda)*L1)+exp(-li*beta2(lambda)*L2)).^2);

% plot, and check if this is as expected:
figure(1);
plot(lambda*1e3, neff1(lambda), 'LineWidth',3); hold on
plot(lambda*1e3, neff2(lambda), 'LineWidth',3); hold off
ax = gca; ax.FontSize = fontsize;
xlabel('λ');
ylabel('Waveguide n_{eff}');
title('Effective Index vs. Input Signal Wavelength for each arm')
grid on

% Plot the actual Response
figure(2);
plot(lambda, T_MZI_nominal(L1, L2, lambda), 'LineWidth',3); hold on
plot(lambda, T_MZI_modulated(L1, L2, lambda), 'LineWidth',3); hold off
ax = gca; ax.FontSize = fontsize;
xlabel ('Wavelength [μm]');
ylabel ('Transmission');
axis tight
title ('MZI transfer function');
xlim(lambda_window)
grid on

figure(3)
t1 = tiledlayout(2,1);

nexttile
% Logarithmic Gain with No Modulation Effect
T_MZI_nominal_dB = 10*log10(T_MZI_nominal(L1, L2, lambda));
plot(lambda, T_MZI_nominal_dB, 'LineWidth',3);
ax = gca; ax.FontSize = fontsize;
xlabel ('Wavelength [μm]');

```

```

ylabel ('Transmission [dB]');
axis tight
text = sprintf('%.0f:%.0f-\mu m Length Mismatch MZI Transfer Function', L1, L2);
title (text);

% Measuring FSRs: We find the indexes of all the minima and
% calculate the difference between them.
localMinIndexes = find(imregionalmin(T_MZI_nominal_dB));
fsrs = diff(1e-6*lambda(localMinIndexes));
fsr = sprintf('FSR: %.2f pm', 1e12*mean(fsrs))

subtitle(fsr)

xlim(lambda_window)
grid on

nexttile
% Logarithmic Gain comparison of Modulation Effect
T_MZI_nominal_dB = 10*log10(T_MZI_nominal(L1, L2, lambda));
T_MZI_modulated_dB = 10*log10(T_MZI_modulated(L1, L2, lambda));
plot(lambda, T_MZI_nominal_dB,'LineWidth',3); hold on
plot(lambda, T_MZI_modulated_dB,'LineWidth',3); hold off
ax = gca; ax.FontSize = fontsize;
xlabel ('Wavelength \lambda [\mu m]');
ylabel ('Transmission [dB]');
axis tight
title ('Shifted MZI transfer function from \beta Modulation');
text = sprintf('Effective Index Difference: %.2f',abs(neff2(lambda0)-neff1(lambda0)));
subtitle(text);
xlim(lambda_window)
grid on
legend('Original', 'Shifted', 'Location','southeast')

```

E. V_π Modelling: Python3

Written by Lukas Chrostowski, November 2021

```

# -*- coding: utf-8 -*-
#####
# Polymer modulator solutions
#####

# configuration: strip waveguide, two metal wires on the side, polymer

# distance between metal electrodes
d = 10e-6
# voltage applied
V = 10
# electric field
E = V/d
# Question

# linear EO coefficient for material
r33 = 20e-12 # m/V; 30 pm/V
# index of refraction
n_eop = 1.6
# change in EO index
dn = -1/2*n_eop**3*r33*E
dndV = -1/2*n_eop**3*r33/d

# confinement
gamma = 0.15

dneff = gamma * dn
# Question

# wavelength

```

```
wvl = 1550e-9

# change in propagation constant
from math import pi
dBeta = dneff*2*pi/wvl

# length
L = 30000e-6

from math import cos
lo = 1/2 * (1+cos(dBeta*L))
# Question

# pi = beta * L = 2*pi/wvl * dn * L
# 1 = 2/wvl / 2*n_eop**3*r_33 * V/d * L
V = wvl / n_eop**3 / r33 * d / L

VpiL = wvl * d / n_eop**3 / (gamma*r33)

VpiLcm = VpiL*100

Vpi = VpiL / L

# e
"""
- same electrode for polling as signal, 2x or more?
- push/pull x2
- increase length
- reduce gap: metal close to WG.
    subject to fabrication risk (small gap, long device)
    subject to optical loss
- more light in the polymer
- reduce width of waveguide:
    - slot
"""
"""

% Finding r33 given dneff
dneff = 0.0003
V = 160
r = 2*dneff/gamma * d / n_eop**3 / V
```

F. MATLAB Measurement Analysis:

```
% Code Originally Provided by Dr. Lukas Chrostowski
% Modified by Davin Birdi, 2021
%
clear
close all
clc

load('L_+100V.mat')
lambda = wavelength;
amplitude = transpose(power(:,1));
dL = 247;

figure(10);
plot(lambda, amplitude)

% Curve fit data to a polynomial for baseline correction
p=polyfit((lambda-mean(lambda))*1e6, amplitude, 4);
```

```

amplitude_baseline=polyval(p,(lambda-mean(lambda))*1e6);

% Perform baseline correction to flatten the spectrum
% Use the curve polynomial, and subtract from original data
amplitude_corrected = amplitude - amplitude_baseline;
amplitude_corrected = amplitude_corrected + max(amplitude_baseline) - max(amplitude);
figure(5);
clf
plot (lambda*1e6, amplitude_corrected);
xlabel ('Wavelength [\mu m]');
ylabel ('Transmission [dB]');
axis tight
title ('Experimental data (baseline corrected)');

% data only within the wavelength range of interest.
lambda_min = min(lambda); % Can limit the analysis to a range of wavelengths
lambda_min = 1.574e-6;
lambda_max = max(lambda); % if the data on the edges is noisy
lambda_max = 1.580e-6;
lambda1=lambda_min:min(diff(lambda)):lambda_max;
amplitude=interp1(lambda, amplitude_corrected, lambda1, 'linear');
lambda=lambda1;
amplitude(find(amplitude==inf))=-50; % check if there are -infinity data points
figure(1);
clf
plot (lambda*1e6, amplitude, 'LineWidth', 1.5);
set(gca, 'FontSize', 12)
xlabel ('Wavelength [\mu m]');
ylabel ('Transmission [dB]');
axis tight
title ('Experimental data (baseline corrected, wavelength range)');

% Define the MZI transfer function
% - as a Taylor expansion around the central wavelength
% - Use units of [microns], which keeps the variables closer to 1.
% - These make the curve fitting easier.
lambda0 = mean(lambda)*1e6;
% use Matlab anonymous functions
% effective index:
neff = @(nx, lambda) ...
    (nx(1) + nx(2).* (lambda-lambda0) + nx(3).* (lambda-lambda0).^2);
% neff([2.4, -1, 0], 1.56) % test it.
% alpha = 1e-3; % propagation loss [micron^-1]
% complex propagation constant
beta = @(nx, alpha, lambda) ...
    (2*pi*neff(nx, lambda)./lambda - 1i*alpha/2*ones(1,length(lambda)) );
% beta([2.4, -1, 0], 1e-3, [1.56, 1.57]) % test it.
% MZI transfer function
T_MZI = @(X, lambda) ...
    (10*log10( 0.25* abs(1+exp(-1i*beta(X(1:3), X(4), lambda)*dL)).^2) +X(5) );
% T_MZI([2.4, -1, 0, 1e-3], [1.56, 1.57]) % test it.

% initial function for fitting
%%%%%%%%%%%%%%%%%%%%%%%%%%%%%%%%%%%%%
nx_init = [2.35, -1, 0]; %%%%%% CHANGE THE FIRST PARAMETER
%%%%%%%%%%%%%%%%%%%%%%%%%%%%%%%%%%%%%
alpha_init = 1e-3; % propagation loss [micron^-1]
x0=[nx_init, alpha_init, 0];
figure(2);
clf
plot (lambda*1e6, amplitude);
hold all;
plot(lambda*1e6, T_MZI(x0, lambda*1e6), 'LineWidth',3);
xlabel ('Wavelength [\mu m]');
ylabel ('Transmission [dB]');
axis tight
title ('MZI model (initial parameters)');

% Curve fit:
[xfit,resnorm] = lsqcurvefit(T_MZI,x0,lambda*1e6,amplitude);
xfit
r=corrcoef(amplitude,T_MZI(xfit, lambda*1e6));
r2=r(1,2).^2

figure(20);
clf
plot (lambda*1e6, amplitude);
hold all;
plot(lambda*1e6, T_MZI(xfit, lambda*1e6), 'LineWidth',3);
xlabel ('Wavelength [\mu m]');
ylabel ('Transmission [dB]');
axis tight
title ('MZI model (fit parameters)');

% Check if the fit is good. If so, find ng
if (ge(r2,0.65))
    % plot ng curve
    figure(4);
    clf
    neff_fit = neff(xfit(1:3),lambda*1e6);
    dndlambd=diff(neff_fit)./diff(lambda); dndlambd=[dndlambd, dndlambd(end)];
    ng=(neff_fit - lambda .* dndlambd);

```

```

plot(lambda*1e6, ng, 'LineWidth', 4);
xlabel ('Wavelength [Nmum]');
ylabel ('Group index, n_g');
axis tight
title ('Group index (from MZI fit)');
ylim([3.75 4])
set(gca, 'FontSize', 12)
% waveguide parameters at lambda0
ng0 = xfit(1) - lambda0*xfit(2)
end

```

IX. TABLE OF TABLES:

Table 1: Variations of Polymer-Optic Modulators to fabricate and Test. All are in unbalanced MZI configurations with length mismatch of ΔL and longer length arm of Max L. They are to be injected with 1550nm wavelength TE optical signal.	3
Table 2: Calculated Performance of Devices. $V\pi$'s calculated using Python Script provided in Appendix, and FSR from MATLAB code also in Appendix.....	3
Table 3: Test Structures on or nearby devices under test used for determining insertion loss and to validate any noise added by fiber array and grating coupler during measurement.....	3
Table 4: Overview of Fabrication Steps followed.....	5
Table 5: Experimental Analysis of Group Index from fit of raw data.	8
Table 6: Effective Index coefficients for Taylor Expansion Polynomial and loss coefficient generated from curve fitting process.	8
Table 7: Simulated Effective Index Parameters from designed device. This was generated using Lumerical MODE	8
Table 8: Effective Indices for Applied Voltages of measured Device, showing a Δn_{eff} of approximately 0.0003.	8

X. TABLE OF FIGURES:

Figure 1: Completed fabricated silicon-photonic chip produced in the Steward Blussom Quantum Matter Institute laboratory with classmates in ELEC463.	1
Figure 2: Example of Length Mismatched MZI designed with the SiEPIC-EBeam-PDK	1
Figure 3: Different effective indices for varied waveguide widths and wavelength sweep, with respective Waveguide Compact Models below. Compact models are derived from Palik using Lumerical MODE with instruction from Dr. Chrostowski [3]. Inset: 220nm by 300nm waveguide signal intensity for TE polarized wave simulated in Lumerical MODE.	2
Figure 4: Example of sinusoidal gain in decibels for (top) 1000 μ m length mismatched MZI, and (bottom) estimated shift of spectrum for an example change in effective index coefficients of waveguide compact model. Both use a 10pm wavelength sweep resolution about the 1550nm wavelength.....	2
Figure 5: Fitted relationship between Electro-optic Coefficient, r_{33} , and Poling Field by Xu et al [1].....	2
Figure 6: Short-1 Device with labelled electrical connections. Both arms of the interferometer are polled, but only from the Probing Terminal to Ground is modulated and affected. This Design can easily create variants with different lengths and mismatches.....	3
Figure 7: Parameters kept constant between designs for this manufacturing run but can be changed for future designs to alter device performance.....	3
Figure 8: Left: Intensity of 1550nm signal in first TE Mode injected into 300nm wide by 220nm tall Si on SiO ₂ waveguide, showing amount of signal outside Silicon waveguide in surrounding material (air) useful for polymer-optic effect. Right: Changes of confinement factor when manufacturing variation such as sloped walls occurs and how this variation can be an advantage with polymer-optic effect.....	4
Figure 9: Full Mask Layout with zoomed area of interest above. Six Polymer-Modulators connected to global Poling Electrodes (top and bottommost metals) and two backup Thermo-Optic Effect Modulators (bottom-left) along with three decoupling test structures (right). Designs optimized for long lengths and small FSRs with variation in waveguide width.....	4
Figure 10: Enlarged view of Short-1 MZI (350 Wide, 1000 Δ L). Annotations denote distances between metal and Silicon features, regions of polling and modulation, and metal connections. Polling occurs in the electric field between VCC and GND, and the modulation only affects polymer between Probing and GND metal connections. All measurements are in micro-meters.....	4
Figure 11: ZEP-EBeam-Process where white is Silicon to keep and grey is Silicon to be etched. The surrounding Silicon has no effect on our devices performance wise and is usually etched away when using a Photolithography process.....	5
Figure 12: Process Cross Sections per procedure that were used to develop a waveguide using the ZEP-E-Beam-Process using the on-site tooling and equipment in Dr. Chrostowski's lab.....	5
Figure 13: Machine settings for PlasmaPro 100 Cobra ICP RIE Etching Machine used for our ZEP-EBeam-Process to dry etch our silicon and electron beam resist.....	6
Figure 14: Metallization Process, starting with high amount of (1) photoresist, (2) lithography, (3) development, (4) Titanium Evaporation Deposition, (5) Gold Evaporation Deposition, (6) and Lift-off Etching. All processes were conducted in SBQMI Clean Room (not to scale).	6
Figure 15: Completed Fabrication Cross Sectional schematic of EO Modulator, viewing modulated arm of MZI (not to scale).....	7
Figure 16: Raw Experimental Data from generated from 100pm resolution wavelength sweep for one device. Red line is a baseline curve fit of the general trend the data is tending towards to remove for correction.	7
Figure 17: Experimental MZI Data modified using baseline-correction to better curve-fit and provide data without noise of grating couplers or insertion loss.	7
Figure 18: Fitted MZI Data for Klose device measured at SBQMI. FSR is extracted using MATLAB 'findpeaks' function.	8
Figure 19: Shifted Spectrum of MZI when applying -60V and 100V to modulation contact pads after poling step. This is limited by the method of how we fit our noisy data and needs to be verified as reproducible using other methods before being considered fully legitimate.	8
Figure 20: Two-Dimensional Corner Analysis of Height and Width of manufactured Waveguide. We can compare our fabricated device with the range of simulated effective indices to gain insight on what device dimensions were fabricated.	9
Figure 21: Example of messy experimental data. Using finer resolution wavelength sweeps can possible aid this to allow better curve fitting.....	9
Figure 22: Revised Design to increase r_{33} by decreasing poling distance from 25 μ m to modulating distance of 8 μ m. Anticipated r_{33} of 100pm/V from our achieved of 60pm/V. Inspired by Liu et. al. [24].....	9
Figure 23: ELEC463 Tuesday Laboratory Section after completing fabrication	10
Figure 24: Programming steps when applying (left) Zep520A EBeam Resists to SOI [9], (center) LOR2A PhotoResist [19], and (right) AZ5214	11